London model allows. The higher the applied field, the more strongly the order parameter is suppressed and the more flux is accumulated in the near-edge layer. On the other hand, when the vortex jumps inside, the screening is restored to a significant extent and, accordingly, there is less flux in the near-edge layer (Fig. 3). The competition between the flux expelled from this layer and the vortex's flux determines the sign and amplitude of flux jumps. Despite the deceptive simplicity of this explanation, there is no simple way to explain why the vortex entry restores screening while the field at the edge remains the same. This is a nonlinear property of superconductors.

We now turn to the question of why the flux jumps are not quantized, even when the surface barrier is suppressed by edge roughness, and why the distance between the curves with and without a vortex is less than ϕ_0 (see Fig. 2). The latter implies that the vortex's flux even in equilibrium (that is, not only the corresponding flux jumps) is considerably less than ϕ_0. This observation can be explained by the changes in the structure of near-edge vortices predicted in refs 1–4. Figure 4 plots the measured amount of flux ϕ carried by a vortex versus its distance from the disk's edge. We can see that all our data for different samples and temperatures fall on a single curve, if plotted in units of the effective penetration length, $\lambda_{eff} = \lambda^2/h$. There is also excellent agreement with the corresponding theoretical dependence. We note that, for a typical experimental situation, h and λ are about 0.1 μm, and it is very unlikely that a vortex can jump farther than 1 μm from the edge before being stopped by pinning, even in samples with low pinning. According to Fig. 4, in such a case the flux carried by vortices is reduced to about $0.5\phi_0$. Only vortices located as far as 100 μm away from the film edge have their flux quantized with an accuracy better than 1%.

We have shown that there are two independent effects that lead to non-quantized penetration of magnetic field in type II superconductors. The first (theoretically established a long time ago, but never observed and often perceived as small) arises due to changes in the structure of near-edge vortices. This should be important in thin films and, in our opinion, may account for a number of unexplained observations. The second, unexpected, effect is more general, and appears owing to the inevitable presence of barriers for flux motion through a superconducting boundary (for example, Bean–Livingston barriers). If such barriers are sufficiently high, nonlinear screening can lead to the extreme situation, causing 'negative vortices'; but if this is not the case, surface barriers can still prevent the quantized penetration. One or both of the above effects can be expected in many—if not most—relevant experimental situations. □

Received 16 June; accepted 12 July 2000.

1. Bardeen, J. Quantization of flux in a superconducting cylinder. *Phys. Rev. Lett.* **7,** 162–163 (1961).
2. Ginzburg, V. L. Magnetic flux quantization in a superconducting cylinder. *Sov. Phys. JETP* **15,** 207–209 (1962).
3. Fetter, A. L. Flux penetration in a thin superconducting disk. *Phys. Rev. B* **22,** 1200–1213 (1980).
4. Kogan, V. G. Pearl's vortex near the film edge. *Phys. Rev. B* **49,** 15874–15878 (1994).
5. White, W. R., Kapitulnik, A. & Beasley, M. R. Collective vortex motion in Mo-Ge superconducting thin films. *Phys. Rev. Lett.* **70,** 670–673 (1993).
6. Fuchs, D. T. *et al.* Transport properties governed by surface barriers in BiSrCaCuO. *Nature* **391,** 373–376 (1998).
7. Geim, A. K. *et al.* Ballistic Hall micromagnetometry. *Appl. Phys. Lett.* **71,** 2379–2381 (1997).
8. Geim, A. K., Dubonos, S. V., Lok, J. G. S., Henini, M. & Maan, J. C. Paramagnetic Meissner effect in small superconductors. *Nature* **396,** 144–146 (1998).
9. Geim, A. K. *et al.* Fine structure in magnetization of individual fluxoid states. *Phys. Rev. Lett.* **85,** 1528–1531 (2000).
10. Schweigert, V. A. & Peeters, P. M. Flux penetration and expulsion in thin superconducting disks. *Phys. Rev. Lett.* **83,** 2049–2052 (1999).
11. Palacios, J. J. Metastability and paramagnetism in superconducting disks. *Phys. Rev. Lett.* **84,** 1796–1799 (2000).

Acknowledgements

We thank V. Kogan for discussions, and FOM, INTAS and NATO for financial support.

Correspondence and requests for materials should be addressed to A.K.G (e-mail: geim@sci.kun.nl).

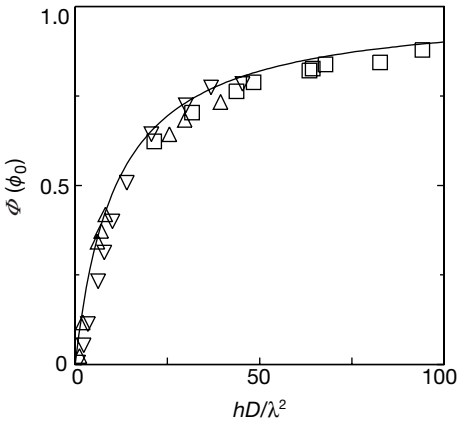

Figure 4 The amount of magnetic flux associated with a vortex in the centre of a thin superconducting disk in equilibrium. The solid curve is an approximate theoretical dependence, $\phi \approx \phi_0\gamma/(\alpha+\gamma)$, found numerically in the limit $h \ll \lambda$, where $\gamma = hD/\lambda^2$ and $\alpha \approx 11.0$ (ref. 3, and V.A.S. *et al.*, manuscript in preparation). Different symbols show experimental data for three disks with D (in μm) ~2 (upright triangles), ~2.4 (inverted triangles) and ~4 (squares), h from about 0.13 to 0.17 μm and the superconducting parameters as in Fig. 2. Because of the surface barrier that is always present (even for a rough edge), we cannot directly determine H_{c1} and, therefore, the amount of flux carried by a vortex in equilibrium. To this end, we notice that the theoretical curves (M–H and Φ–H) for $L = 0$ and 1 are nearly parallel below H_{c1} (Fig. 3) and, hence, the amount of flux associated with vortex exit is sufficiently close—within our experimental uncertainty of 10%—to the vortex's flux in equilibrium. So we have measured the amplitude of flux jumps for the vortex exit. To obtain different data points for each of the disks, we varied the penetration length (T) by changing the temperature from 0.4 K to close to $T_C \approx 1.25$ K. No fitting parameters were used, except for a slight adjustment (≤10%) of the absolute scale along the ϕ axis for each of the disks.

Nanomechanical oscillations in a single-C_{60} transistor

Hongkun Park*‡§, Jiwoong Park†, Andrew K. L. Lim*, Erik H. Anderson‡, A. Paul Alivisatos*‡ & Paul L. McEuen†‡

* *Department of Chemistry and* † *Department of Physics, University of California at Berkeley and* ‡ *Materials Sciences Division, Lawrence Berkeley National Laboratory, Berkeley, California 94720, USA*

The motion of electrons through quantum dots is strongly modified by single-electron charging and the quantization of energy levels[1,2]. Much effort has been directed towards extending studies of electron transport to chemical nanostructures, including molecules[3–8], nanocrystals[9–13] and nanotubes[14–17]. Here we report the fabrication of single-molecule transistors based on individual C_{60} molecules connected to gold electrodes. We perform transport measurements that provide evidence for a coupling between the centre-of-mass motion of the C_{60} molecules and single-electron hopping[18]—a conduction mechanism that has not been observed previously in quantum dot studies. The coupling is manifest as quantized nano-mechanical oscillations of the C_{60} molecule against the gold surface, with a frequency of about 1.2 THz. This value is in good agreement with a simple theoretical

§ Present address: Department of Chemistry and Chemical Biology, Harvard University, Cambridge, Massachusetts 02138, USA.

estimate based on van der Waals and electrostatic interactions between C_{60} molecules and gold electrodes.

Single-C_{60} transistors were prepared by depositing a dilute toluene solution of C_{60} onto a pair of connected gold electrodes fabricated using electron-beam lithography. A break-junction technique[11] was then used to create a gap between these electrodes by the process of electromigration. The typical lateral size of the fabricated electrodes was of the order of 100 nm at the point of the gap formation, and the height of the electrodes was 15 nm. Scanning electron microscope images of fabricated electrodes reveal that the gap between two electrodes is not uniform and that the narrowest gap is formed only between small protrusions ($\leq$10 nm) of two gold electrodes. Current–voltage measurements[11] of these electrodes at cryogenic temperatures without deposited C_{60} molecules show that the size of the gap is consistently about 1 nm. In a significant fraction of the C_{60} devices, the conductance of the junction after initial breaking is substantially enhanced compared to devices with no C_{60} deposited, indicating that C_{60} molecules reside in the junction. The entire structure was defined on a SiO_2 insulating layer on top of a degenerately doped silicon wafer that serves as a gate electrode that modulates the electrostatic potential of C_{60}. A schematic diagram of an idealized single-C_{60} transistor is shown in the lower inset of Fig. 1.

Figure 1 presents representative current–voltage (I–V) curves obtained from a single-C_{60} transistor at different gate voltages (V_g). The device exhibited strongly suppressed conductance near zero bias voltage followed by step-like current jumps at higher voltages. The voltage width of the zero-conductance region (conductance gap) could be changed in a reversible manner by changing V_g. In ten devices prepared from separate fabrication runs, the conductance gap could be reduced to zero by adjusting V_g, although the gate voltage at which the conductance gap closed (V_c) varied from device to device.

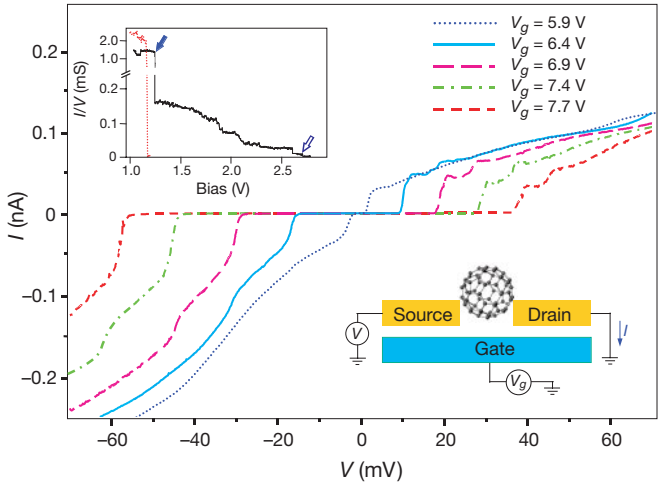

Figure 1 Current–voltage (I–V) curves obtained from a single-C_{60} transistor at T = 1.5 K. Five I–V curves taken at different gate voltages (V_g) are shown. Single-C_{60} transistors were prepared by first depositing a dilute toluene solution of C_{60} onto a pair of connected gold electrodes. A gap of $\sim$ 1 nm was then created using electromigration-induced breaking of the electrodes. Upper inset, a large bias was applied between the electrodes while the current through the connected electrode was monitored (black solid curve). After the initial rapid decrease (solid arrow), the conductance stayed above $\sim$0.05 mS up to $\sim$2.0 V. This behaviour was observed in most single-C_{60} transistors, but it was not observed when no C_{60} solution was deposited (red dotted curve). The bias voltage was increased until the conductance fell low enough to ensure that the current through the junction was in the tunnelling regime (open arrow). The low bias measurements shown in the main panel were taken after the breaking procedure. Lower inset, an idealized diagram of a single C_{60}-transistor formed by this method.

Figures 2 and 3 show two-dimensional plots of differential conductance ($\partial I/\partial V$) as a function of both V and V_g for four different devices. Peaks in $\partial I/\partial V$, which correspond to the step-like features in Fig. 1, show up as lines in these plots. As seen clearly in Figs 2 and 3, the size of the conductance gap and the $\partial I/\partial V$ peak positions evolve smoothly as V_g is varied. As the gate voltage was varied farther away from V_c in both positive and negative directions, the conductance gap continued to widen and the maximum observed gap exceeded 270 mV. Many $\partial I/\partial V$ peaks outside the conductance gap are also observed.

The V_g-dependent features described above were not observed in devices when C_{60} was not deposited on the electrodes. In addition, the coverage of C_{60} on the electrodes was such that only about 10% of more than 300 fabricated electrodes show I–V characteristics that are different from a simple tunnel junction without C_{60}. This low C_{60} coverage ensures that the probability of finding multiple C_{60} molecules bridging two electrodes is small. Furthermore, many different devices exhibited similar conductance characteristics that are consistent with a single nanometre-sized object bridging two electrodes, as explained in detail below[1]. Although C_{60} could not be imaged directly in these devices because of its small size ($\sim$7 Å in diameter), these experimental observations indicate that individual C_{60} molecules are responsible for the conductance features observed in the experiment.

The global patterns observed in Figs 1–3 can be understood using ideas borrowed from the Coulomb blockade model developed for the analysis of quantum-dot transport[1]. The conductance gap observed in the data is a consequence of the finite energy required to add (remove) an electron to (from) C_{60}. This energy cost arises from the combined effect of single-electron charging of C_{60} and the quantized excitation spectrum of the C_{60}-transistor system. The maximum observed gap in the experiment indicates that the charging energy of the C_{60} molecule in this geometry can exceed 270 meV.

The conductance gap changes reversibly as a function of V_g because a more positive gate voltage stabilizes an additional electron

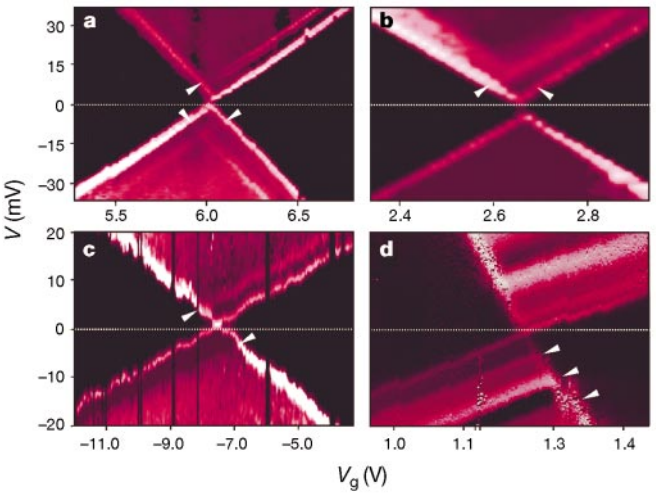

Figure 2 Two-dimensional differential conductance ($\partial I/\partial V$) plots as a function of the bias voltage (V) and the gate voltage (V_g). Data were obtained from four different devices prepared from separate fabrication runs. The dark triangular regions correspond to the conductance gap, and the bright lines represent peaks in the differential conductance. **a**–**d**, The differential conductance values are represented by the colour scale, which changes from black (0 nS) through pink to white (white representing 30 nS in **a**, **b** and **c** and 5 nS in **d**). The white arrows mark the point where $\partial I/\partial V$ lines intercept the conductance gap. During the acquisition of data in **d**, one 'switch' where the entire $\partial I/\partial V$ characteristics shift along the V_g axis occurred at V_g = 1.15 V. The right portion of the plot **d** is shifted along the V_g axis to preserve the continuity of the lines.

on C_{60}. The conductance gap disappears at $V_g = V_c$ where the total energy of the system is the same for two different C_{60} charge states. When the gate voltage traverses V_c in the positive direction, the equilibrium number of charges on C_{60} changes by one electron from C_{60}^{n-} to $C_{60}^{(n+1)-}$, where n designates the number of charges on C_{60}. It is determined by both V_g and the local electrochemical environment, that is, the work function of the metal electrode and the local charge distribution around C_{60}. While the value of n cannot be determined solely from our experimental data, previous electrochemical and photoelectron spectroscopic studies of C_{60} on gold suggest that n is most likely to be zero or one[19].

The position of each $\partial I/\partial V$ peak outside the conductance gap in Figs 2 and 3 provides detailed information on the quantized excitations of the single-C_{60} transistor system[1]. These $\partial I/\partial V$ peaks appear when a new quantized excitation becomes energetically accessible, providing an electron-tunnelling pathway between C_{60} and the gold electrodes. Specifically, each $\partial I/\partial V$ peak on the $V_g < V_c$ side signifies an opening of a new tunnelling pathway where an electron hops onto C_{60}^{n-} to generate $C_{60}^{(n+1)-}$ in its ground or excited states; these peaks therefore probe the excitation energies of the $C_{60}^{(n+1)-}$ ion. Each $\partial I/\partial V$ peak that appears at $V_g > V_c$ occurs when an electron hops off $C_{60}^{(n+1)-}$ to generate C_{60}^{n-}; these peaks thus probe the ground and excited states of C_{60}^{n-}. The energy of these quantized excitations can be determined from the bias voltage at which they intercept the conductance gap[1], as shown by the white arrows in Fig. 2.

A remarkable common feature of the different devices is that a quantized excitation is universally observed with an energy of approximately 5 meV. Moreover, this excitation is observed on both sides of V_c in most devices, indicating that it is an excitation of both charge states of C_{60}. The exact value of this energy quantum varied from device to device and ranged from 3 to 7 meV. In some devices, multiple $\partial I/\partial V$ features with almost identical spacing appear, as seen in Fig. 2d.

The observed 5-meV excitation could arise from many possible degrees of freedom of the single-C_{60} transistor system. One possibility, which has often been invoked in other nanometre-scale systems, is the excited electronic states of the system. However, this possibility is highly unlikely here because the 5-meV excitation is the same for both charge states of C_{60} and also because multiple excitations with the same spacing are observed. Although the exact electronic-level structures of the C_{60}^{n-} ions are not known experimentally, theoretical calculations predict that the electronic states do not follow such behaviour[19,20].

A more natural candidate is a vibrational excitation of the C_{60} system coupled to an electron tunnelling on and off C_{60}. The observation of multiple $\partial I/\partial V$ features with identical spacing would then result from the excitation of integer numbers of vibrational quanta. Moreover, these vibrational modes would be present irrespective of the charge state of the C_{60}.

The internal vibrational modes of the free C_{60} molecule have been extensively studied, both theoretically and experimentally[19,21]. The lowest-energy mode is one with a vibrational quantum of 33 meV and corresponds to the C_{60} deformation from a sphere to a prolate ellipsoid, as shown in the inset to Fig. 3. In Fig. 3, an excitation that probably corresponds to this mode can indeed be seen with an energy of about 35 meV. However, internal vibrational modes cannot account for the observed 5-meV features.

Another possibility is the centre-of-mass oscillation of C_{60} within the confinement potential that binds it to the gold surface, as shown in Fig. 4. To our knowledge, this mode has not been directly measured experimentally. However, previous theoretical and experimental studies have shown that C_{60} is held tightly on gold by van der Waals interactions, with a C_{60}–gold binding energy of about 1 eV and a distance of about 6.2 Å between the C_{60} centre and the gold surface[19,22,23]. Assuming that the C_{60}–gold interaction potential can be expressed by the Lennard–Jones form[23], the above parameters can be used to determine the shape of the potential that describes the C_{60}–gold binding. This calculation indicates that the C_{60}–gold binding near the equilibrium position can be approximated very well by a harmonic potential with an estimated force constant of $k \approx 70\ \mathrm{N\,m^{-1}}$, as is shown schematically in Fig. 4. This force constant and the mass M of the C_{60} molecule yield a vibrational frequency of $f = 1/2\pi(k/M)^{1/2} \approx 1.2$ THz and a vibrational quantum of $hf \approx 5$ meV, where h is the Planck constant.

Adding an additional electron to C_{60} compresses the C_{60}–surface bond due to the interaction between the C_{60} ion and its image charge in the metal. A simple estimate indicates that an additional electron on C_{60} results in the shortening of the C_{60}–surface distance by $\delta \approx 4$ pm, but it does not significantly change the vibrational

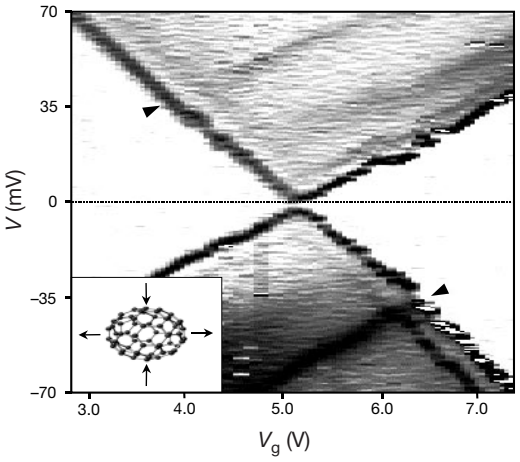

Figure 3 A differential conductance plot showing a larger bias-voltage range than those in Fig. 2. Here two $\partial I/\partial V$ lines that intercept the conductance gap at $V = 35$ mV are seen clearly (arrows). The energy quantum of this excitation closely matches that of the C_{60} internal vibrational mode shown in the inset.

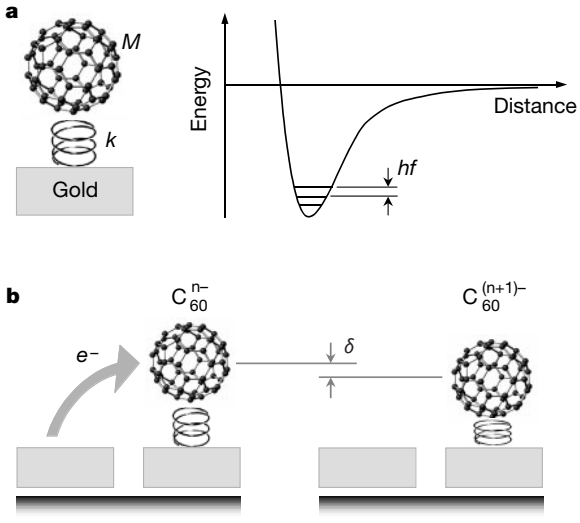

Figure 4 Diagram of the centre-of-mass oscillation of C_{60}. **a**, A C_{60} molecule is bound to the gold surface by the van der Waals and electrostatic interaction. The interaction potential is shown schematically alongside. The potential near the equilibrium position can be approximated well by a harmonic potential with a force constant k. This harmonic potential gives quantized energy levels with frequency $f = 1/2\pi(k/M)^{1/2}$. Here M represents the mass of C_{60} and h is the Planck constant. **b**, When an electron jumps on to C_{60}^{n-}, the attractive interaction between the additional electron and its image charge on gold pulls the C_{60} ion closer to the gold surface by the distance δ. This electrostatic interaction results in the mechanical motion of C_{60}.

frequency. By comparison, the r.m.s. (root mean square) displacement x_m of the C_{60} molecule in the mth vibrational level is given by $x_m = (2m+1)^{1/2}x_0$, where $x_0 = (hf/k)^{1/2} \approx 3\,\mathrm{pm}$. Although the exact values of these simple estimates change when the second metal electrode is included in the model, the qualitative conclusions of the model remain essentially the same. The present estimates pertain to the situation where the coupling between C_{60} and two electrodes is strongly asymmetric.

The C_{60}–surface vibration discussed above can account for the 5-meV conductance features in a unifying fashion. The first $\partial I/\partial V$ peak at the boundary of the conductance-gap region is observed when an electron hops on or off C_{60} with the system staying in the ground vibrational level. Additional $\partial I/\partial V$ peaks on the $V_g < V_c$ side appear when an electron hops onto C_{60}^{n-} to generate $C_{60}^{(n+1)-}$ in excited vibrational states. The $\partial I/\partial V$ peaks on the $V_g > V_c$ side signify, on the other hand, an event where an electron hops off $C_{60}^{(n+1)-}$, leaving C_{60}^{n-} in excited vibrational levels. Multiple $\partial I/\partial V$ peaks on the same side of V_c indicate that multiple vibrational quanta are excited.

This process is thus reminiscent of the Franck–Condon processes encountered in electron-transfer and light-absorption processes in molecules, where the vibrational excitation accompanies the electronic motion[24]. Within the harmonic approximation, the vibrational matrix elements for these processes can readily be calculated, and the ratio δ/x_0 determines the number of vibrational quanta typically excited by the tunnelling electron. According to the estimates discussed above, $\delta/x_0 \approx 1$ in a single-C_{60} transistor. The number of $\partial I/\partial V$ peaks visible in Fig. 2 in general confirms this expectation as only a few $\partial I/\partial V$ peaks are observed in most devices.

One device that does not follow this general trend is the one shown in Fig. 2d. As described previously, this device exhibits many $\partial I/\partial V$ peaks on both sides of V_c. In addition, the peak intensities do not show the simple variations expected from the single-mode Franck–Condon situation[24]. The anomalous behaviour may be related to the highly asymmetric coupling of C_{60} and the two electrodes in this particular device. This asymmetry is demonstrated by the different slopes of the upward and downward $\partial I/\partial V$ lines in the V–V_g plane. The variations of peak intensities may be due to the presence of other degrees of freedom in the system, such as the C_{60} motion perpendicular to the surface normal.

Unexplained features exist in other devices as well. In the data in Fig. 2a, a small (≤ 1 meV) energy splitting is observed for many of the lines. This splitting may arise from the C_{60} centre-of-mass motion perpendicular to the surface normal discussed above. Unfortunately, the nature of the potential for this motion is not known, owing to the lack of detailed knowledge of the electrode geometry near C_{60}, and quantitative support of this assignment is thus lacking at present.

The transport measurements presented here demonstrate that single-electron-tunnelling events can be used both to excite and probe the motion of a molecule: indeed, the single-C_{60} transistor behaves as a high-frequency nanomechanical oscillator. Furthermore, the oscillations of the C_{60} molecule must be treated in a quantized fashion, showing that this is a true quantum 'mechanical' system. We expect that the coupling between the quantized electronic and mechanical degrees of freedom will be generically important in electron transport through nanomolecular systems[25,26]. □

Received 17 March; accepted 30 June 2000.

1. Grabert, H. & Devoret, M. H. *Single Charge Tunneling* (Plenum, New York, 1992).
2. Sohn, L. L., Kouwenhoven, L. P. & Schön, G. *Mesoscopic Electron Transport* (Kluwer Academic, Dordrecht, 1997).
3. Bumm, L. A. *et al.* Are single molecular wires conducting? *Science* **271,** 1705–1707 (1996).
4. Reed, M. A., Zhou, C., Muller, C. J., Burgin, T. P. & Tour, J. M. Conductance of a molecular junction. *Science* **278,** 252–254 (1997).
5. Datta, S. *et al.* Current-voltage characteristics of self-assembled monolayers by scanning tunneling microscopy. *Phys. Rev. Lett.* **79,** 2530–2533 (1997).
6. Porath, D., Levi, Y., Tarabiah, M. & Millo, O. Tunneling spectroscopy of isolated C_{60} molecules in the presence of charging effects. *Phys. Rev. B* **56,** 9829–9833 (1997).
7. Joachim, C. & Gimzewski, J. K. An electromechanical amplifier using a single molecule. *Chem. Phys. Lett.* **265,** 353–357 (1997).
8. Stipe, B. C., Rezaei, M. A. & Ho, W. Single-molecule vibrational spectroscopy and microscopy. *Science* **280,** 1732–1735 (1998).
9. Klein, D. L., McEuen, P. L., Bowen Katari, J. E., Roth, R. & Alivisatos, A. P. An approach to electrical studies of single nanocrystals. *Appl. Phys. Lett.* **68,** 2574–2576 (1996).
10. Klein, D. L., Roth, R., Lim, A. K. L., Alivisatos, A. P. & McEuen, P. L. A single-electron transistor made from a cadmium selenide nanocrystal. *Nature* **389,** 699–701 (1997).
11. Park, H., Lim, A. K. L., Park, J., Alivisatos, A. P. & McEuen, P. L. Fabrication of metallic electrodes with nanometer separation by electromigration. *Appl. Phys. Lett.* **75,** 301–303 (1999).
12. Banin, U., Cao, Y., Katz, D. & Millo, O. Identification of atomic-like electronic states in indium arsenide nanocrystal quantum dots. *Nature* **400,** 542–544 (1999).
13. Kim, S.-H., Medeiros-Ribeiro, G., Ohlberg, D. A. A., Williams, R. S. & Heath, J. R. Individual and collective electronic properties of Ag nanocrystals. *J. Phys. Chem. B* **103,** 10341–10347 (1999).
14. Bockrath, M. *et al.* Single-electron transport in ropes of carbon nanotubes. *Science* **275,** 1922–1925 (1997).
15. Tans, S. J. *et al.* Individual single-wall carbon nanotubes as quantum wires. *Nature* **386,** 474–477 (1997).
16. Tans, S. J., Verschueren, A. R. M. & Dekker, C. Room-temperature transistor based on a single carbon nanotube. *Nature* **393,** 49–52 (1998).
17. Bockrath, M. *et al.* Luttinger-liquid behaviour in carbon nanotubes. *Nature* **397,** 598–601 (1999).
18. Gorelik, L. Y. *et al.* Shuttle mechanism for charge transfer in Coulomb blockade nanostructures. *Phys. Rev. Lett.* **80,** 4526–4529 (1998).
19. Dresselhaus, M. S., Dresselhaus, G. & Eklund, P. C. *Science of Fullerenes and Carbon Nanotubes* (Academic, New York, 1996).
20. Green, W. H. Jr *et al.* Electronic structures and geometries of C_{60} anions via density functional calculations. *J. Phys. Chem.* **100,** 14892–14898 (1996).
21. Heid, R., Pintschovius, L. & Godard, J. M. Eigenvectors of internal vibrations of C_{60}: Theory and experiment. *Phys. Rev. B* **56,** 5925–5936 (1997).
22. Chavy, C., Joachim, C. & Altibelli, A. Interpretation of STM images: C_{60} on the gold (110) surface. *Chem. Phys. Lett.* **214,** 569–575 (1993).
23. Ruoff, R. S. & Hickman, A. P. Van der Waals binding of fullerenes to a graphite plane. *J. Phys. Chem.* **97,** 2494–2496 (1993).
24. Schatz, G. C. & Ratner, M. A. *Quantum Mechanics in Chemistry* (Prentice Hall, Englewood Cliffs, 1993).
25. Poncharal, P., Wang, Z. L., Ugarte, D. & De Heer, W. A. Electrostatic deflections and electromechanical resonances of carbon nanotubes. *Science* **283,** 1513–1516 (1999).
26. Reulet, B. *et al.* Bolometric detection of mechanical bending waves in suspended carbon nanotubes. Preprint cond-mat/9907486 at ⟨http://xxx.lanl.gov⟩ (1999).

Acknowledgements

We thank M. S. Fuhrer and N. S. Wingreen for discussions and advice. This work was supported by the US Department of Energy. E.A. was also partially supported by DARPA.

Correspondence and requests for materials should be addressed to P.M. (e-mail: mceuen@socrates.berkeley.edu).

Gas-phase production and photoelectron spectroscopy of the smallest fullerene, C_{20}

Horst Prinzbach*, Andreas Weiler*, Peter Landenberger*, Fabian Wahl*, Jürgen Wörth*, Lawrence T. Scott†, Marc Gelmont†, Daniela Olevano‡ & Bernd v. Issendorff ‡

* *Institut für Organische Chemie und Biochemie, Albert-Ludwigs-Universität, 79104 Freiburg, Germany*
† *Department of Chemistry, Boston College, Merkert Chemistry Center, Chestnut Hill, Massachussetts 02467-3860, USA*
‡ *Fakultät für Physik, Albert-Ludwigs-Universität, 79104 Freiburg, Germany*

Fullerenes are graphitic cage structures incorporating exactly twelve pentagons[1]. The smallest possible fullerene is thus C_{20}, which consists solely of pentagons. But the extreme curvature and reactivity of this structure have led to doubts about its existence and stability. Although theoretical calculations have identified, besides this cage, a bowl and a monocyclic ring isomer as low-energy members of the C_{20} cluster family[2], only ring isomers of C_{20} have been observed[3–6] so far. Here we show that the cage-structured fullerene C_{20} can be produced from its perhydrogenated form (dodecahedrane $C_{20}H_{20}$) by replacing the hydrogen atoms